Lake Level Change From Satellite Altimetry Over Seasonally Ice-Covered Lakes in the Mackenzie River Basin

Yuande Yang, Philip Moore, Zhenhong Li, and Fei Li

***Abstract*— Variations in water levels of seasonally ice-covered subarctic lakes are indicators of environmental and climatic change. Satellite altimetry enables remote sensing of these lakes, but the lake phenology is problematic as radar reflection surfaces include water, snow, and ice. Reflection from multiple surfaces gives rise to two-peak waveforms across ice-covered lakes. Misinterpretation of the altimetric height has caused extracted water levels to be low compared with gauge data. In this study, a modified retracker is used to determine heights from the first altimetric subwaveform. Using *in situ* snow depth and ice thickness, the first reflection surface is shown to correspond closely to the snow/ice interface when the lake is frozen. The modified retracker is applied to the Great Bear Lake (GBL), Great Slave Lake (GSL), and Lake Athabasca (ATL) of the Mackenzie River Basin for the period 1992–2020. Standard deviations (Std) of differences between lake levels from Jason-2 waveforms and *in situ* data across GBL and GSL are 0.06 m with the new methodology compared with 0.11 and 0.08 m, respectively, using the standard Ice retracker. With an Std of 0.11 m between altimetric and gauge lake levels, TOPEX/Poseidon is less accurate than the combined Jason missions (Std: 0.07 m).**

***Index Terms*— Lake level, Mackenzie River basin, reflection surface, satellite altimetry, seasonal ice-covered lake.**

I. Introduction

LAKE level change is significant for environmental studies, global climate research, and the planning and management of regional resources [1]–[5]. *In situ* observations can monitor lake level variations, but the number of gauges has declined since the 1980s, with gauges unavailable in many Asian and African countries [6]. For the Arctic and subarctic lakes, the scarcity of continuous *in situ* monitoring has constrained spatiotemporal evaluation in response to climate variability. Although primarily conceived to measure sea level, satellite altimetry has an established capability for inland water and cryospheric studies [7]–[9]. Altimetry has been used over inland waters since the 1990s to monitor lakes, wetlands, rivers, and reservoirs. In one of the earliest studies, Morris and Gill [10] monitored water level changes in the Great Lakes. The success of altimetry in inland water has led to the development of databases that focus on large basins and major rivers, such as the Mekong and Amazon [11]–[14]. However, as noted in [13]–[15], inland water is more problematic than open oceans and seas. In particular, altimeter missions will not overfly all inland waters, with small water bodies missed by repeat pass missions due to the across-track spacing of the ground tracks. Over smaller water bodies, the waveforms are often complex and compound due to various reflectors within the footprint; the typical 20-Hz waveform data may suffer from pointing issues as the ground points are spaced about 330 m apart along-track for nadir pointing altimeters. Satellite altimetry can also lose lock while the altimeter fails to adjust to rapidly changing topography along the ground track [16]. In terms of height extraction from radar altimetry, the standard oceanic Brown waveform model is generally not applicable over inland waters. A single-peak specular waveform is not untypical over large rivers and lakes. To extract oceanic and inland water levels, waveform retrackers have been developed to improve the accuracy of the range from the satellite to reflector [14]–[20]. For ice-covered lakes in the Arctic and subarctic, there is a further complexity due to multiple altimetric reflection surfaces. Snow crystals, snow density, ice lenses, and liquid water content are factors affecting reflection from snow, while the density and size of air bubbles within the ice layer the dominant parameters for ice reflection [21]. Thus, the interpretation of the reflection surface is a challenge in using satellite radar altimetry to retrieve ice-covered lake levels. Ricko *et al.* [22] reported erroneously large differences between altimetric and *in situ* heights during ice-covered seasons for Mackenzie Basin lakes, noting a difference of 1.69 m in 1995 for Lake Athabasca (ATL).

However, change in the nature of the reflection surface causes temporal variations in the waveform characterization. It has been shown [21] that satellite altimetric waveforms exhibit double peaks during the ice-covered seasons in Arctic lakes, which can then be used to retrieve ice thickness.

Manuscript received August 27, 2020; revised October 27, 2020; accepted November 17, 2020. Date of publication December 9, 2020; date of current version September 27, 2021. This work was supported in part by the National Key Research and Development Program of China under Grant 2018YFC1406103, in part by the National Natural Science Foundation of China under Grant 42076234 and Grant 41941019, in part by the Fundamental Research Funds for the Central Universities, CHD, under Grant 300102260301/087 and Grant 300102260404/087, in part by the China Scholarship Council under Grant 201806275009, in part by U.K. Natural Environment Research Council (NERC) through the Centre for the Observation and Modelling of Earthquakes, Volcanoes and Tectonics (COMET) under Grant come30001, in part by WeACT Project under Grant NE/S005919/1, and in part by European Space Agency through the ESA-MOST DRAGON-5 Project under Grant 59339. *(Corresponding author: Yuande Yang.)*

Yuande Yang and Fei Li are with the Chinese Antarctic Center of Surveying and Mapping, Wuhan University, Wuhan 430079, China (e-mail: yuandeyang@whu.edu.cn; fli@whu.edu.cn).

Philip Moore is with the School of Engineering, Newcastle University, Newcastle upon Tyne NE1 7RU, U.K. (e-mail: philip.moore@newcastle.ac.uk).

Zhenhong Li is with the College of Geological Engineering and Geomatics, Chang'an University, Xi'an 710054, China, and also with the Key Laboratory of Western China's Mineral Resource and Geological Engineering, Ministry of Education, Xi'an 710054, China (e-mail: zhenhong.li@chd.edu.cn).

This article has supplementary material provided by the authors and color versions of one or more figures available at https://doi.org/10.1109/TGRS.2020.3040853.

Digital Object Identifier 10.1109/TGRS.2020.3040853

Double-peaked waveforms are ideally suited for subwaveform (SW) analysis. Such analyses are proven to be beneficial in subdividing the waveform, enabling focus on the waveform component across gates pertinent to a particular reflection signature. SW retracking has been used in coastal regions [20] and across rivers and lakes [23]–[25]. Failure to consider the presence of multipeaks partly explained the errors in [22]. In that study, heights were extracted from the assumed leading edge on the basis that the waveform exhibited a single peak rather than a compound waveform with reflections from multiple surfaces. Similar results are seen in this article when an SW retracker is utilized in an initial comparison of altimetric and *in situ* lake levels heights. The altimetric lake levels are lower than *in situ* heights during ice-covered seasons as the retracker focuses on the dominant second peak of the waveform. To retrieve ice-covered lake levels, a modified SW retracker is applied. The double-peak SW is further divided into two component subwaveforms (CSWs). Examination of the offsets among the reflection surfaces, namely, the air–snow, snow–ice, and ice–water interfaces, enables water levels to be recovered from the first CSW. The procedure is applied to the three largest lakes of the Mackenzie River Basin to determine lake level time series from 1992 to 2020.

This article is structured as follows. Section II introduces the study area and data sets employed within the analysis. The methodology is introduced in Section III. Section IV examines the possible reflection surfaces using *in situ* ice thickness and snow depth data, confirming that the recovered lake levels correspond closely to the snow–ice interface in the ice seasons. Using results from the previous sections, the time series of lake levels is presented in Section V and compared against *in situ* gauge data. Conclusions are presented in Section VI.

II. Study Area and Data Sets

A. Study Area

ATL (area 7900 km^2), Great Slave Lake (GSL, 28 568 km^2), and Great Bear Lake (GBL, 31 328 km^2) of the Mackenzie River Basin (see Fig. 1) are selected to investigate lake level variations. The temperatures range between −50 °C and 30 °C, with a typical −30 °C to −25 °C in winter and 15 °C to 20 °C in summer. There is a strong precipitation gradient within the Mackenzie River Basin with annual precipitation exceeding 1000 mm in southwest mountainous areas, decreasing to 300 mm in the northeast [26], [27].

B. Data

1) Altimetric Data: The TOPEX/Poseidon (T/P) altimeter mission series, including T/P and Jason-1/2/3, are utilized to derive lake levels over ATL, GSL, and GBL. The principle of satellite altimetry is shown in Fig. 2. These satellite missions have a repeat ground track of 9.92 days. With an inclination of 66°, the subsatellite ground tracks cover ATL and GSL but only partially cover GBL due to its location beyond the northern limit of the orbit. Altimetric data are extracted from Sensor Geophysical Data Records (SGDRs), over the period 1992–2002, 2002–2009, 2008–2017, and 2016–2019 for T/P and Jason-1/2/3, respectively. The details of the SGDR retrackers and data providers are given in Table I. SGDRs contain

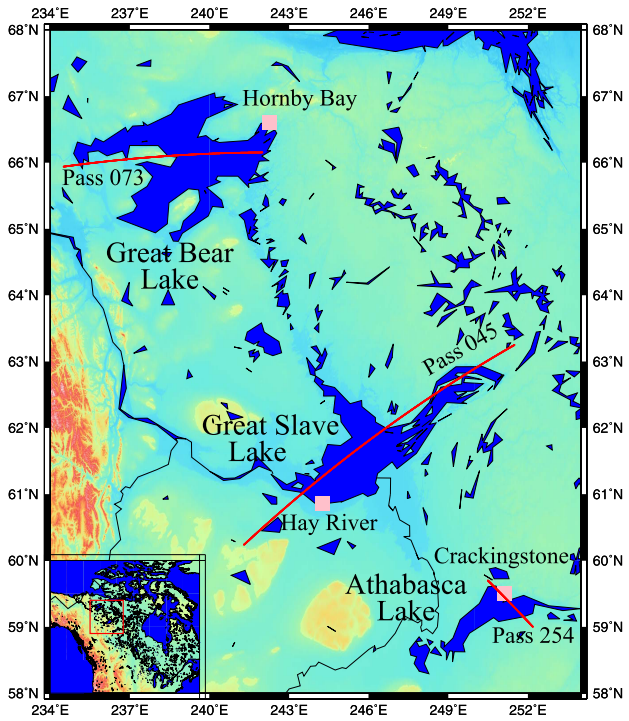

Fig. 1. Location of the study area, T/P passes, and pressure gauge locations.

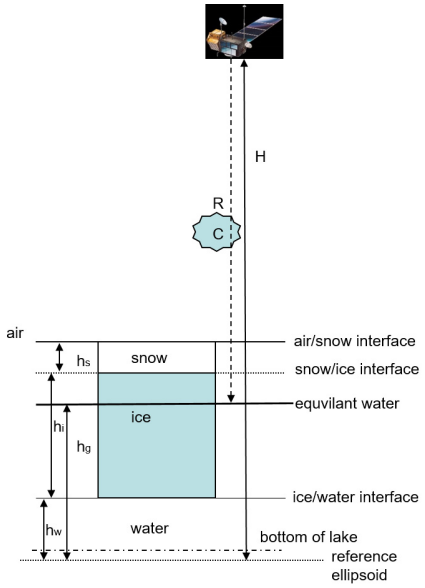

Fig. 2. Principle of satellite altimetry over ice-covered lakes.

the satellite altitude, raw range, heights from retrackers, instrumental corrections, ionospheric, wet and dry tropospheric corrections, other geophysical corrections (e.g., solid Earth tides), and T/P 10-Hz and Jason 20-Hz waveforms. As onboard radiometers are saturated by brightness temperatures over land, the European Centre for Medium-Range Weather Forecasts (ECMWF) modeled tropospheric delay is applied [13].

2) Lake Level Observations: Lake gauge data were collected by the environment and natural sources of Canada (https://www.canada.ca/en/services/environment). In this study, data from Cracking Stone (ATL), Hay River (GSL), and Hornby Bay (GBL) are utilized with locations shown in Fig. 1. Data are from January 1992 to December 2017 for

TABLE I
T/P AND JASON ALTIMETRY

Mission	SGDR version	SGDR Retrackers	Time span	Provider
T/P	MGDR-B	#	1992-2002	PODAAC
Jason-1	E	MLE4, Ice	2002-2012	Aviso
Jason2	D	MLE3, MLE4, Ice	2008-2017	Aviso
Jason3	D	MLE3, MLE4, Ice	2016-2019	Aviso

ATL and GSL and January 1992 to December 2016 for GBL. For lake level monitoring, environment and natural resources employ either submersible pressure transducers or pressure purge systems connected to a transducer on the shore. Both types rest on the lake bottom near the shoreline attached either by an air tube (pressure purge system) or electric cable (submersible transducer) and measure hydrostatic pressure of the water column above the sensor (Randy Wedel, private communication). With ice cover, this also includes the weight of the ice and snow as part of the water column. The data from the transducers are converted to a water level relative to a vertical datum connected to the Canadian Geodetic Vertical Datum 2013, CGVD2013a. Despite ice cover conditions during the winter months, the water levels fluctuate in response to wind and differences in barometric pressure, which results in variable seiche effects observed in real-time data. By using daily averaging, the seiche effects will be minimized. *In situ* data are collected at near shoreline locations, often in bays, and, thus, potentially present a different ice environment to more open lake altimetric conditions. The difference in the ice environment may give rise to water level differences at the cm level or higher (Randy Wedel, private communication).

3) Ice Thickness and Snow Depth Data: Weekly *in situ* ice thickness measurements, from drill holes on GSL near Yellowknife, are collected by the Canadian Ice Thickness Program (CITP) of the Canadian Ice Service. Data for the months November to May from 2002 onward are available for the ice season (https://www.canada.ca/en/environment-climate-change/services/ice-forecasts-observations/latest-conditions/archiveoverview/thickness-data.html). Snow depth is available in the same site.

III. METHODOLOGY

A. Seasonally Ice-Covered Lakes: Altimetric Waveforms

CryoSat-2 altimetric waveforms exhibit double peaks during ice-covered seasons in Arctic lakes [21]. We show the annual change in the waveform composition for conventional nadir pointing altimeters by reference to the T/P mission series. Fig. 3 shows the temporal variation of GSL waveforms from Jason-2 pass 045 (see Fig. 1). Fig. 3 presents waveform profiles on June 15 (late ice melt) and 25 and November 11 (open water) and December 11 (early ice season) in 2009. In 2010, January 10 and March 10 are mid-season ice, April 9 late-season ice, April 19 early ice melt, and May 28 ice melt. The specular waveform of Fig. 3(a), with its high singular peak, sharp decline, and low power in the tail, is indicative

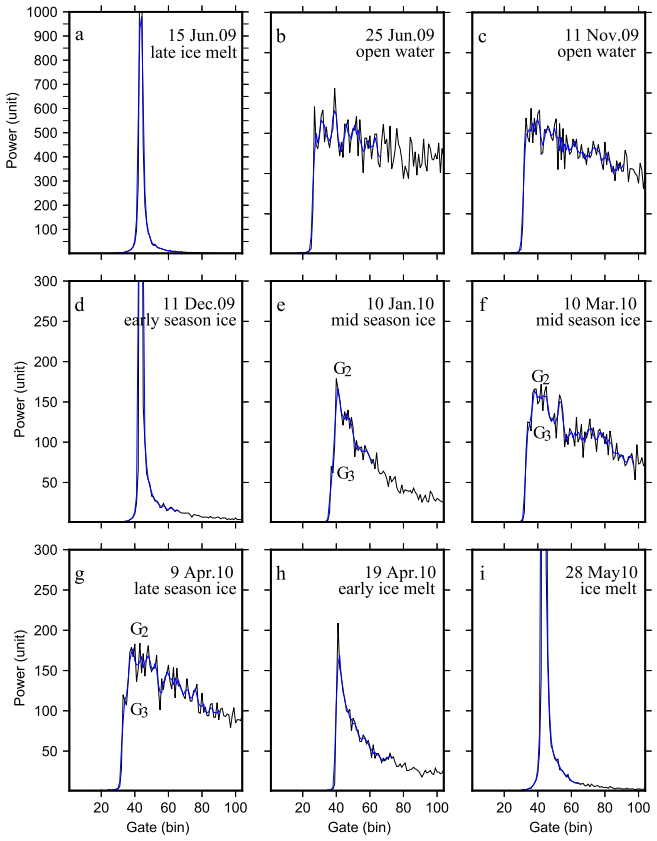

Fig. 3. Temporal variation of GSL Jason-2 pass 045 waveforms (black curve) with smoothed waveforms on (a) Jun 15, 2009; (b) Jun 25, 2009; (c) Nov 11, 2009; (d) Dec 11, 2009; (e) Jan 10, 2010; (f) Mar 10, 2010; (g) Apr 9, 2010; (h) Apr 19, 2010; and (i) May 28, 2010.

of scattering from flat ice or meltwater on an ice surface. Fig. 3(b) and (c) shows single-diffuse-peak waveforms that are typical reflections from open water. The high power in the tail is due to surface roughness and off-nadir reflections as observed in oceanic returns. An early ice season waveform is given in Fig. 3(d). Fig. 3(d) is similar to Fig. 3(a) but with different powers in the tail. Two peaks separated by a number of range gates are observed in Fig. 3(e). These peaks represent differential scattering from interfaces among air, snow, ice, and water in the early lake ice growth season. The same peaks can be seen in Fig. 3(f) and (g), with an increasing range gate difference, indicating reflections from thicker ice in the later ice growth season. Fig. 3(h) is similar to Fig. 3(d), but from early ice melt. Fig. 3(i) is almost the same as Fig. 3(a), indicating similar reflections. Waveforms for T/P, Jason-1, and Jason-3, are given in Figs. S1–S3 in the Supplementary Material.

For seasonally ice-covered lakes, the vertical distribution of air, snow, ice, and water is shown in Fig. 2, leading to the actual waveforms (see Figs. 3 and 4) characterized by two peaks separated by a number of gates (equivalent to offset in vertical height) during ice seasons, as shown in the CryoSat-2 waveforms [21]. However, there are differences between the T/P family (see Figs. 3 and S1–S3) and CryoSat-2, as the power of the first peak is smaller than the second for the T/P family, while the CryoSat-2 peaks are of similar amplitude. CryoSat-2 operates in one of three modes: the pulse-limited low-resolution mode (LRM) that is the same

as the T/P family, synthetic aperture radar (SAR) mode, and interferometric SAR mode (SARin) [28]. Over the lakes considered, CryoSat-2 operated in the SARin mode. In the SARin mode, the left antennas transmit bursts of coherent radar pulses with the reflected pulse received by the left and right antennas. Interferometry allows inference of surface slope. The SARin processing strategy is the same as SAR with the bursts directed into narrow beams directed at ground points approximately 300 m apart [29]. The SAR/SARin waveforms have different characteristic shapes over oceans and inland waters to the LRM of CryoSat-2 and T/P family of missions. For all satellites, waveforms with two or more peaks during the ice-seasons can be subdivided into SWs, as air/snow, snow/ice, and/or ice/water provide separate components of the waveforms.

B. SW Threshold Retracking

The SGDRs provide lake heights from three retrackers: MLE3, MLE4, and Ice [30]. However, none of these trackers are designed or tuned for ice-covered lakes; particularly, the two-peak waveforms observed during the ice seasons. This study develops a modified SW approach for two-peak waveforms during the ice seasons. For all waveforms, we first extract an SW that is retracked using the OCOG/Threshold retracker [31] to obtain the height corresponding to a point on the leading edge. We refer to this step as subwaveform threshold (ST) retracking. For waveforms with double peaks, a modified retracking method is adopted in which two CSWs, each containing a peak, are extracted. The leading edge from the first CSW is used to calculate the range correction and, hence, derive the lake level. Processing of the CSW using the OCOG/Threshold retracker is called the modified subwaveform threshold (MST) retracker to distinguish it from the ST retracker.

1) ST Retracking: Theory: This section builds on [32] and presents details of SW retracking applicable to waveforms collected in ice-covered lakes. In this approach, a four-parameter standard waveform is based on the Brown model

$$P(t) = 0.5A\left[\text{erf}\left((t-\tau)/\left(\sqrt{2}\sigma\right)\right)+1\right] \times \begin{cases} 1, & t < \tau \\ \exp(-(t-\tau)/\alpha), & t \geq \tau \end{cases} \quad (1)$$

where $P(t)$ is the power at the gate corresponding to time t, A is the amplitude, erf is the error function, τ is the center of the leading edge, σ is the slope of the leading edge, and α is a decay parameter. The standard leading edge with 22 samples is calculated from the Brown model shown in Fig. 4(a), using *a priori* values of four parameters [30]. The sample size of 22 is adequate to capture the leading edge and is equivalent to over 10 m in height using the conversion factor 0.46875 m/gate [30]. This standard waveform is subsequently used to obtain the actual leading edge of the waveform, G_f, to end gate G_e in Fig. 4(b). The search for the leading edge is facilitated by taking consecutive 22 gate waveforms starting with gates 1–22, with the last subset from gates $N-21$ to N, forming a total of $N-21$ subsets. N is 64 for T/P and 104 for Jason. The correlation coefficient between the standard leading edge in Fig. 4(a) and each subset forms a series of $N-21$ values. The correlation coefficient series between Fig. 4(a) and (b) is plotted in Fig. 4(c). The SW identified for retracking has a starting gate at the maximum (G_f) correlation in Fig. 4(c) with gates G_f–G_e encompassing the leading edge [32]. The OCOG/Threshold retracker provides the time, t_1, or, equivalently, the gate of the retracked point G_R. Typically, this yields a single retracked point on the leading edge.

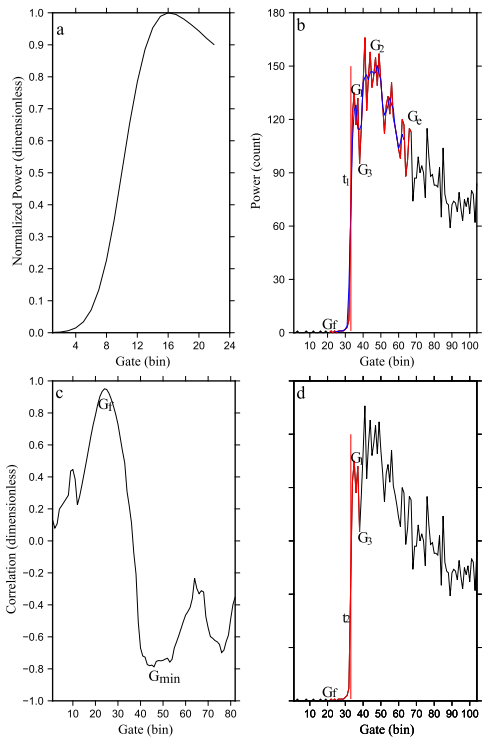

Fig. 4. (a) Standard leading edge from the Brown model. (b) SW retracking gates (red curve) and smoothed waveform (blue). (c) Correlation coefficient time series. (d) Modified SW retracking.

The retracked point $G_R(t_1)$ is used to obtain the height correction

$$\text{Cr} = 0.46875(G_R - G_T) \quad (2)$$

where G_T is the default leading-edge gate, and as stated previously, the factor 0.46875 converts gate to distance (m). For the T/P family of altimetric missions, $G_T = 32$.

2) Altimetric Lake Level: Theory: As shown in Fig. 2, the orthometric lake level, L, is the difference between the satellite height and the corrected range

$$L = H - R - \text{Geoid} - C \quad (3)$$

where H is the satellite altitude above the reference ellipsoid, R is the raw altimetric range, Geoid is the geoid height, and C denotes the total correction

$$C = \text{Cload} + \text{Csolid} + \text{Cpole} + \text{Cion} + \text{Cdry} + \text{Cwet} + \text{Cins} + \text{Cr}. \quad (4)$$

From left to right, the terms on the right-hand side in (4) are corrections for load tide, solid earth tide, pole tide, ionospheric

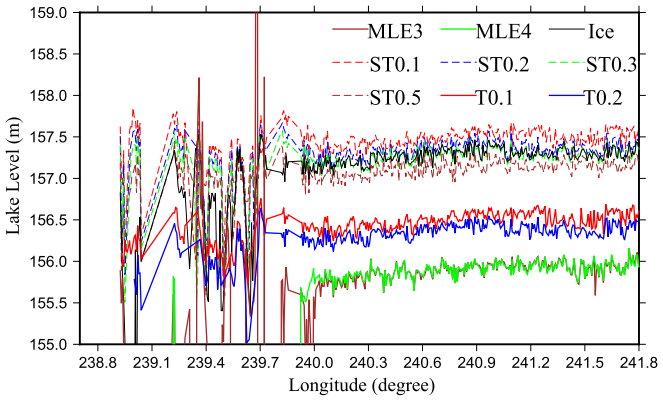

Fig. 5. Along-track GBL retracked lake levels: Jason-2 cycle 0 pass 073; MLE3, MLE4, T0.1, and T0.2 offset by −1 m.

TABLE II

STATISTICS OF AVERAGE LAKE LEVELS BETWEEN RETRACKED JASON-2 HEIGHTS AND IN SITU DATA: PASS 073, CYCLE 0 OVER GBL FOR LONGITUDES BETWEEN 240.3 °E AND 241.8 °E

Retracker	Mean(m)	Std(m)
ST0.1	157.50	0.07
ST0.2	157.38	0.07
ST0.3	157.30	0.08
ST0.5	157.15	0.08
T0.1	157.49	0.07
T0.2	157.36	0.07
ICE	157.30	0.07
MLE3	156.91	0.08
MLE4	156.91	0.08

delay, dry and wet tropospheric delays, instrumental corrections, including Doppler, the center of gravity, and so on, and the waveform retracking range correction (2).

3) Altimetric Lake Level (ST Retrackers): As an example, we apply the ST retracker with various threshold values to extract along-track GBL lake levels between 238.9 °E and 241.8 °E for Jason-2 pass 073 of cycle 0 (July 4, 2008). The satellite ground track is close to its maximum latitudinal extent with the satellite moving from west to east. Jason-2 SGDR data provide along-track retracked lake levels using the Ice, MLE3, and MLE4 retrackers (see Fig. 5). The MLE3 and MLE4 retrackers are noisy as the satellite transitions from land to water, perhaps due to residual ice; July 4 is during the melt season. To avoid this effect, Table II summarizes statistics of retracked 20-Hz lake levels between 240.3 °E and 241.8 °E; outliers exceeding three-sigma are removed.

As raw/retracked measurements are reduced to an orthometric height, the averaged height from the retracked 20-Hz heights, as in ocean studies, can reduce the uncertainty. The standard deviation (Std) of Table II represents the noise in the 20-Hz data although geophysical signatures (e.g., seiche effects) could contribute. Even with the restricted longitudinal range, the ice retracker is more precise than the oceanic MLE3 and MLE4 over inland waters. Threshold and ST retrackers are of similar precision over open water, for a given threshold value. Fig. 5 also shows the heights from threshold retracker (T) with threshold values 0.1 and

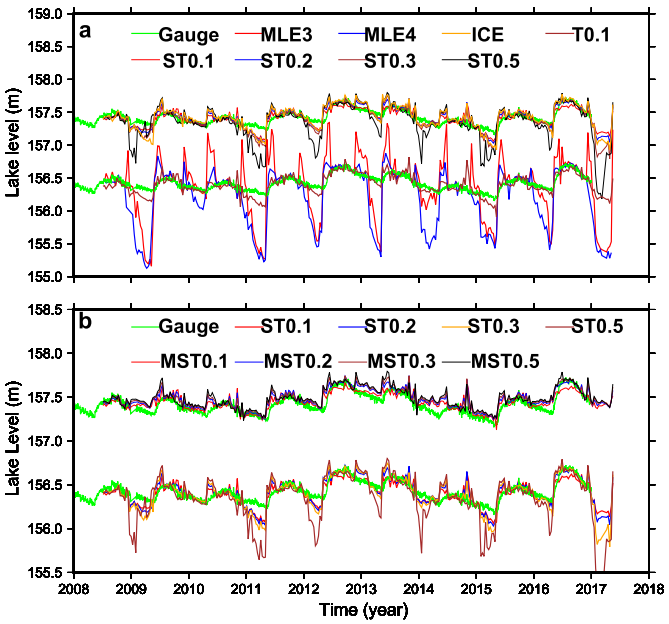

Fig. 6. GBL lake level time series from Jason-2 pass 073. (a) Gauge, SGDR, T, and ST retrackers; lake levels from MLE3, MLE4, and T0.1 shift down 1 m. (b) Gauge, ST, and MST retrackers; lake levels from ST retrackers offset down 1 m.

0.2 and the ST retracker using threshold values of 0.1, 0.2, 0.3, and 0.5 with statistics in Table II. The analysis shows the improvement of Stds with lower threshold values in T and ST retrackers. Signatures in the western part of the lake are, as noted previously, probably related to residual ice. For example, the average retracked water level from T0.1 is 157.14 and 157.51 m over 239.4 °E–239.7 °E and 240.0 °E–241.8 °E, respectively, with corresponding values 157.15 and 157.35 m for ST0.1. The average ST0.1 lake levels over 240.0 °E–241.0 °E and 241.0 °E–241.8 °E (after removing outliers) are 157.33 and 157.37 m. Fig. 5 also shows the differences in offsets among the retrackers. Such differences are systematic as the retracked gate moves with the retracker. For example, the T and ST retracked points move to lower gate numbers with a decrease in threshold value as the retracked point moves down the leading edge.

Differences between the mean values of retracked heights from Pass 073 in the GBL and *in situ* gauge are plotted in Fig. 6. Fig. 6(a) shows the results after removing the offset, with statistics in Table III. Again, the ice retracker outperforms MLE3 and MLE4. For the ST retrackers, a threshold value of 0.1 shows the best fit to the *in situ* data. However, as shown in Fig. 6, altimetric heights during the ice-covered seasons (September–July) are suboptimal with lower values than the gauge data.

C. MST Retracking: Theory

With reference to Fig. 4(a), the ST retracker identifies the SW from G_f to G_e. As observed in Fig. 4, the extracted SWs are two-peaked during ice-covered seasons, with lake levels from ST lower than gauge data as the retracked heights are biased by the second and higher waveform peak. MST retracking seeks to extract heights from the first component of the two-peak SW for comparison against gauge data. Fig. 4(b) shows the two SW components from G_f to G_3 and G_3 to

TABLE III
STATISTICS OF LAKE LEVEL DIFFERENCES BETWEEN RETRACKED JASON-2 PASS 073 AND IN SITU DATA OVER GBL

Retracker	#	Offset (m)	Max (m)	Min (m)	Mean (m)	Std (m)
ST0.1	306	0.07	0.30	-0.19	0.01	0.08
ST0.2	306	-0.08	0.27	-0.21	0.00	0.09
ST0.3	306	-0.18	0.26	-0.28	-0.01	0.10
ST0.5	306	-0.33	0.28	-0.67	-0.05	0.19
T0.1	306	0.10	0.40	-0.29	-0.02	0.09
ICE	306	-0.18	0.33	-0.30	-0.01	0.11
MLE3	301	-0.58	0.95	-1.15	-0.02	0.39
MLE4	268	-0.58	0.45	-1.18	-0.20	0.38
MST0.1	306	0.07	0.32	-0.11	0.03	0.06
MST0.2	306	-0.08	0.32	-0.07	0.06	0.06
MST0.3	306	-0.18	0.33	-0.06	0.07	0.06
MST0.5	306	-0.33	0.30	-0.12	0.07	0.07

G_e where G_3 is the local minimum between peaks G_1 and G_2. To extract the first CSW, a modified approach is used. First, the SW is extracted as previously using correlations across a 22 gate span. The SW is subsequently smoothed to reduce speckle error and accentuate the local maxima and minima, as shown in Fig. 4(b). Here, we use a moving average of three gate values. Two local maxima are observed in the smoothed SW, corresponding to gates G_1 and G_2, with gate G_3 corresponding to the local minimum between G_1 and G_2. Fig. 3 shows smoothed SWs in blue, with the second and dominant peak, G_2, clear in each two-peak waveform. The lower peak, G_1, is less distinct with the minimum, G_3, identified through the waveform slope negative between G_3-1 and G_3 and positive between G_3 and G_3+1. Finally, the first CSW from G_f to G_3 [see Fig. 4(b) and (d)] is retracked from the actual waveform with the chosen threshold value and point t_2 calculated.

The MST retracker with the various threshold values has been applied to pass 073 across GBL, pass 045 across GSL, and pass 245 across ATL. Fig. 6(b) shows the GBL lake level time series from the gauge and the T, ST, and MST approaches. In contrast to the T and ST heights, the results with MST are closer to the *in situ* data over ice-covered seasons. Table III summarizes the results. All MST retrackers exhibit enhanced agreement with a threshold value of 0.1, yielding an Std of 0.06 m to the gauge data. Analogous results for passes across GSL and ATL are given in Figs. S4 and S5 and Tables S1 and S2 in the Supplement Material. Altimetric heights across all lakes demonstrate that the MST yields closer agreement to the gauge heights than T, ST, and SGDR retrackers with a capability to track the *in situ* pressure gauge data in ice cover seasons.

IV. VALIDATION OF REFLECTION SURFACE CORRESPONDING TO FIRST CSW

A. Theoretical Considerations

As shown in Fig. 2, the gauge height is recovered from the weight of the equivalent water column above the pressure sensor, namely, a combination of water, ice, and snow load. As the previous section established good agreement between *in situ* and altimetric heights during ice cover, the first CSW reflection surface could correspond closely to the air/snow, snow/ice, or ice/water interface. Validation of this reflection surface is undertaken to utilize snow depth and ice thickness data available during the winter seasons.

For a pressure gauge, the equivalent water height (level) is

$$h_g = h_w + h_i\rho_i/\rho_w + h_s\rho_s/\rho_w \tag{5}$$

where ρ_w, ρ_i, and ρ_s are the densities of water, ice, and snow, respectively, and h_g, h_w, h_i, and h_s the gauge height, water height, ice thickness, and snow depth. Taking ρ_w, ρ_i, and ρ_s as 1000, 920, and 200 kg $\cdot$ m^{-3}, respectively, h_g becomes

$$h_g = h_w + 0.92h_i + 0.20h_s. \tag{6}$$

Previous studies [21] and [33] established that radar penetrates dry snow but is reflected from wet snow. For the air/snow interface, the theoretical altimetric height $h_w + h_i + h_s$ is the sum of snow, ice, and water, and hence, the theoretical lake level difference between the altimetric height and gauge height, h_g, is

$$LD_a = 0.08h_i + 0.80h_s. \tag{7}$$

For reflection from the snow/ice interface, the theoretical altimetric height is $h_w + h_i$, and

$$LD_s = 0.08h_i - 0.20h_s \tag{8}$$

while, for the ice/water interface, the theoretical altimetric height is h_w, and

$$LD_i = -0.92h_i - 0.20h_s. \tag{9}$$

Equations (7)–(9) formulize the dependence of the pressure gauge and altimetric height differences on ice and snow cover. The gauge height is less than the altimetric height for an air/snow reflection surface and greater than for the ice/water interface (see Fig. 2), assuming a constant velocity of the radar through the mediums. This assumption is correct for the air/snow interface, but, for the snow/ice interface, the orthometric height correction due to change of velocity through snow is

$$LD_{sv} = -h_s(1/ns - 1) = 0.113h_s \tag{10}$$

on using $ns = 1.1271$ [34] as the Ku-band refractive index of snow. Similarly, for reflection from the snow/ice interface, the orthometric height correction due to the radar velocity change in ice and snow is

$$LD_{iv} = -h_s(1/ns - 1) - h_i(1/ni - 1) = 0.113h_s + 0.440h_i \tag{11}$$

where $ni = 1.7861$ [35] is the Ku-band refractive index of ice.

Weekly GSL snow depth and ice thickness data from 2002 to 2017 are available from Yellowknife (see Fig. 7). The summary statistics in Table IV show maximum ice thickness and snow depth of 1.46 and 0.46 m, with an average of 0.81 and 0.19 m, respectively. Using the weekly data, theoretical lake level differences between altimetry and gauge derived from (7)–(11) are plotted as Fig. 8(a) with statistics summarized in Table V. If the surface is air/snow, altimetric results are larger than the *in situ* heights, ranging from 0.01 to 0.44 m, with an average 0.20 m. However, altimetric results are about -1.15 m lower than the situ data for the ice/water interface, ranging between -2.03 and -0.28 m. For snow/ice,

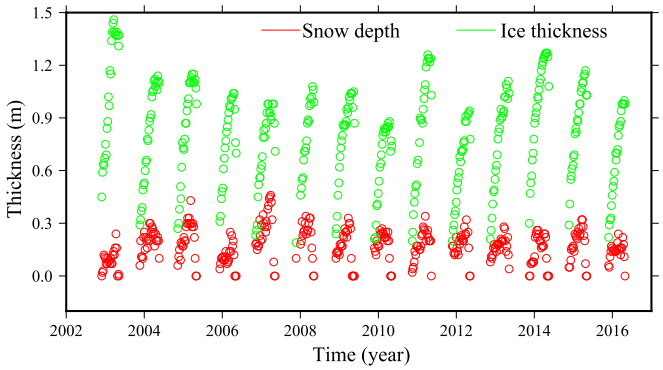

Fig. 7. GSL ice thickness and snow depth.

TABLE IV
YELLOWKNIFE SNOW DEPTH AND ICE THICKNESS: SUMMARY STATISTICS (cm)

	Min	Max	Average
Snow	1	46	18.98
Ice	19	146	80.57

TABLE V
ICE SEASON GSL THEORETICAL LAKE LEVEL DIFFERENCES BETWEEN ALTIMETRIC REFLECTION SURFACES AND PRESSURE GAUGE. $(\text{ALT-GAUGE})^{\text{ice}}$ VALUES ARE MST0.1 DIFFERENCES TO GAUGE DURING ICE SEASON (NOVEMBER–MAY)

Surface	#	Max (m)	Min (m)	Mean (m)	Std (m)
air/snow	347	0.44	0.02	0.20	0.08
snow/ice	347	0.11	-0.07	0.01	0.03
ice/water	347	-0.28	-2.03	-1.15	0.40
$(\text{Alt-gauge})^{\text{ice}}$	347	0.19	-0.14	0.01	0.05

the difference depends on snow depth and ice thickness, varying between −0.07 and 0.11 m. The air–snow interface leads to excessive altimetric heights, while the ice–water interface results in low altimetric heights during the ice seasons. Table V also shows that correction for the ice-snow reflection surface has a minimal impact with Std 0.03 m.

B. Reflection Surface: Validation

Differences between altimetric and gauge measurements at the weekly ice season epochs from November to May are given in Table V. These values show that correction for the theoretical air/snow or ice/water interfaces will have a positive or negative impact, and only the snow/ice correction can be positive or neutral. This inference is further investigated by subtracting the theoretical GSL lake level differences [see Fig. 8(a)] from altimetric MST0.1 altimetric heights. The modified lake levels are compared with the pressure gauge data in Fig. 8. Results, with/without corrections for the air/snow, snow/ice and ice/water reflection surfaces, are summarized in Table VI. In Fig. 8(b) and Table VI, the gauge data are interpolated to the altimetric epochs, including a zero correction during June–October when the ice thickness is not recorded. During these months, the lake will be open water or covered by thin ice. Table VI reveals that the correction for

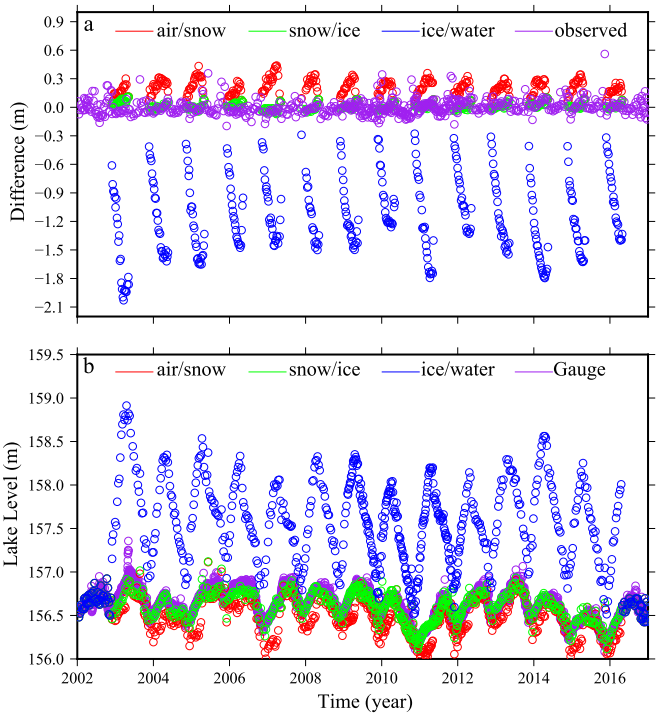

Fig. 8. (a) Observed MST0.1 GSL ice season variation and theoretical lake level differences between altimetric and pressure gauge data for various reflection surfaces. (b) GSL pressure gauge heights and corrected MST0.1 lake level time series with respect to different reflection surfaces.

TABLE VI
COMPARISONS OF ALTIMETRIC AND IN SITU DATA WITH/WITHOUT CORRECTIONS FOR AIR/SNOW, SNOW/ICE, AND ICE/WATER REFLECTION SURFACES

Surface	#	Max (m)	Min (m)	Mean (m)	Std (m)
Uncorrected	910	0.49	-0.29	0.01	0.09
air/snow	910	0.49	-0.47	-0.14	0.11
snow/ice	910	0.55	-0.21	-0.02	0.08
ice/water	910	2.01	-0.08	0.97	0.40

snow/ice reflection surface enhances the uncorrected heights to provide the lowest Std, but that correction for the snow/ice surface has only a marginal effect. However, the positive impact of the snow/ice interface correction confirms that the retracked lake levels from the first CSW should correspond closely to the snow/ice surface as seen with CryoSat-2 [21].

V. LAKE LEVELS: MULTIMISSION RESULTS

The previous section establishes that uncorrected lake levels from MST0.1 during open water and ice cover are very close to the equivalent water height. Correction to the pressure gauge for the snow/ice interface in (8) requires *in situ* snow depth and ice thickness data. In addition, the modified velocity of the radar pulse through snow also requires snow depth. Using a 0.20-m snow depth and 0.80-m ice thickness (see Table IV), the snow correction equates to −0.016 m in (8) and almost cancels with the +0.023 m in (10). The ice correction from the same snow depth and ice thickness is −0.78 m in (9) and 0.37 m in (11). Snow depth is a more readily available parameter, but the ice thickness measurements are not routinely available for GBL and ATL. Accordingly, our

TABLE VII

STATISTICS OF LAKE LEVEL DIFFERENCES BETWEEN ALTIMETRIC (MST0.1) AND IN SITU DATA OVER ATL, GSL, AND GBL FOR T/P FAMILY MISSIONS

Lake	Sat	#	Offset (m)	Max (m)	Min (m)	Mean (m)	Std (m)
ATL	T/P	276	2.43	0.76	-0.59	0.07	0.17
	J1	310	0.30	0.34	-0.27	0.02	0.07
	J2	300	1.13	0.37	-0.31	-0.05	0.08
	J3	64	0.93	0.20	-0.23	-0.06	0.09
	All	907		0.54	-0.59	0.01	0.12
GSL	T/P	321	2.00	0.40	-0.52	0.03	0.11
	J1	356	-0.22	0.36	-0.20	-0.01	0.08
	J2	310	0.47	0.56	-0.13	0.03	0.06
	J3	69	0.33	0.17	-0.16	-0.02	0.06
	all	910		0.49	-0.29	0.01	0.09
GBL	T/P	283	1.55	0.49	-0.24	0.04	0.11
	J1	338	-0.86	0.32	-0.28	0.01	0.07
	J2	306	0.07	0.32	-0.11	0.03	0.06
	J3	69	-0.03	0.04	-0.16	-0.06	0.06
	All	1013		0.56	-0.52	0.01	0.08

approach is to ignore the snow/ice interface correction and to utilize the MST0.1 heights as a close approximation to the equivalent water height across GBL and ATL in the ice seasons. Table VI show that such an approach is acceptable for GSL. This approach is used to derive lake level time series for GBL, GSL, and ATL and enables the methodology to be generalized to other ice-covered lakes where ice thickness data is unavailable or uncertain.

Applying the MST retracker with the 0.1 threshold value, we derive lake level time series for ATL, GSL, and GBL from T/P and Jason-1/2/3. Based on the comparisons between altimetry and gauge, we derive the offset between *in situ* and altimetry for the three lakes. The results are shown in Table VII. Large offsets are observed. Each altimetric mission has a so-called altimeter bias due to an electronic delay, while the differences between the gauge datum and the SGDR geoid may introduce further uncertainty. It is noted that, using GSL as an example, there is minimal offset for Jason-1. However, the altimetric lake level is 2.00 and 0.47 m higher than the gauge value for T/P and Jason-2. Normalizing for the offsets, lake level time series of ATL, GSL, and GBL from T/P and Jason-1/2/3 are plotted in Fig. 9. There are no obvious differences between altimetry and gauge data over both ice-free and ice-covered seasons, indicating the consistency between the gauge and altimetric lake level. Table VII summarizes the statistics between altimetric and gauge lake levels of Fig. 9. There are larger differences between T/P and the gauge data compared with the Jason missions, indicating an improvement in altimetry with time. Agreement between T/P for 1996–98 and Jason-2 for 2016 is noticeably worse over GBL. Overall, the Std of the Jason series is 0.08, 0.06, and 0.06 m for ATL, GSL, and GBL, respectively, increasing to 0.12, 0.09, and 0.08 m after adding T/P. The poorer performance of T/P is also seen over individual lakes, for example, the Std of the differences in ATL is 0.17 m for T/P but reduces to 0.07, 0.08, and 0.09 m with Jason-1/2/3. Moreover, GSL and GBL reveal better agreements than ATL for all missions, implying

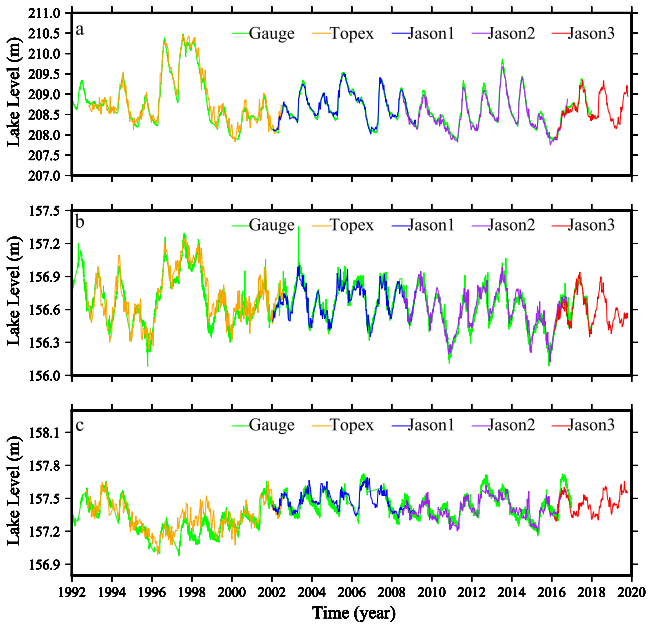

Fig. 9. Lake level time series from T/P family and gauge. (a) ATL. (b) GSL. (c) GBL.

the size of the lake or the distance to the shore affects the accuracy.

VI. CONCLUSION

This study considers the temporal variation of water levels for the three largest lakes in the Mackenzie River Basin. The changes in the T/P family of waveforms throughout the year are associated with the nature of the reflecting surface (water–ice, water, ice, and snow–ice). The SW retracker with threshold 0.1 has proved to derive lake levels of marginally better accuracy than the SGDR retrackers. However, these retrackers derive lower lake levels than gauged heights during ice-covered seasons. Two-peak waveforms are observed in the ice-covered lakes for all T/P family altimetric missions. An MST retracker resolves the height discrepancy, where the first CSW is retracked to derive the lake level.

GSL snow depth and ice thickness are used to calculate the theoretical lake level differences between altimetric and *in situ* data for different reflection surfaces relative to the equivalent water height of a pressure gauge. Calculations show that the corrected altimetric height is larger than the gauge values for the air/snow interface and smaller for the ice/water interface. Corrections for the snow/ice interface have lower Std than the uncorrected differences. Applying these corrections shows that the snow/ice interface correction marginally improves the overall results. However, the improvement is sufficiently small to permit the uncorrected altimetric heights to be utilized for lakes without *in situ* ice thickness data. It is crucial that the results establish that the altimetric reflection surface of the first CSW is close to the snow–ice boundary.

The lake level time series using MST0.1 is close to the *in situ* measurements over GBL, GSL, and ATL during all seasons. The Std of lake level differences between the Jason series and the *in situ* data is 0.08, 0.06, and 0.06 m for ATL, GSL, and GBL, increasing to 0.12, 0.09, and 0.08 m after adding T/P altimetric results.

The proposed retracking algorithm improves the accuracy of altimetry heights and opens up the possibility of determining global lake water levels from archived satellite altimetry data, including T/P and Jason, the ERS and ENVISAT missions, CryoSat-2, and Sentinel-3. Retracking of the second SW facilitates the determination of lake ice thickness, which is the subject of a future study.

ACKNOWLEDGMENT

The authors thank the anonymous reviewers who have provided very constructive comments. They sincerely thank the Canadian Ice Service for providing ice thickness and ice cover data, AVISO for Jason Sensor Geophysical Data Record (SGDR) data, and PODAAC for the TOPEX/Poseidon (T/P) SGDR data.

REFERENCES

[1] L. C. Brown and C. R. Duguay, "The response and role of ice cover in lake-climate interactions," *Prog. Phys. Geography Earth Environ.*, vol. 34, no. 5, pp. 671–704, Oct. 2010.

[2] Z. Long, W. Perrie, J. Gyakum, D. Caya, and R. Laprise, "Northern lake impacts on local seasonal climate," *J. Hydrometeorol.*, vol. 8, no. 4, pp. 881–896, Aug. 2007.

[3] S. Stitt, J. L. Dwyer, D. G. Dye, and E. G. Josberger, "Terrestrial essential climate variables at a glance," U.S. Geological Surv. Sci. Invest. Map, Reston, VA, USA, Tech. Rep. 2011-3155, 2011.

[4] F. Lenormand, C. R. Duguay, and R. Gauthier, "Development of a historical ice database for the study of climate change in Canada," *Hydrol. Processes*, vol. 16, no. 18, pp. 3707–3722, Dec. 2002.

[5] K. K. Pour, C. R. Duguay, A. Martynov, and L. C. Brown, "Simulation of surface temperature and ice cover of large northern lakes with 1-D models: A comparison with MODIS satellite data and in situ measurements," *Tellus A, Dyn. Meteorol. Oceanogr.*, vol. 68, no. 1, p. 17614, 2012.

[6] C. Vörösmarty *et al.*, "Global water data: A newly endangered species," *EoS, Trans. Amer. Geophys. Union*, vol. 82, no. 5, pp. 54–58, Jan. 2001.

[7] J. Ziyad, K. Goïta, R. Magagi, F. Blarel, and F. Frappart, "Improving the estimation of water level over freshwater ice cover using altimetry satellite active and passive observations," *Remote Sens.*, vol. 12, no. 6, p. 967, Mar. 2020.

[8] Y. B. Sulistioadi *et al.*, "Satellite radar altimetry for monitoring small rivers and lakes in Indonesia," *Hydrol. Earth Syst. Sci.*, vol. 19, no. 1, pp. 341–359, Jan. 2015.

[9] K.-C. Cheng, C.-Y. Kuo, H.-Z. Tseng, Y. Yi, and C. K. Shum, "Lake surface height calibration of Jason-1 and Jason-2 over the Great Lakes," *Mar. Geodesy*, vol. 33, no. 1, pp. 186–203, Aug. 2010.

[10] C. S. Morris and S. K. Gill, "Evaluation of the TOPEX/Poseidon altimeter system over the Great Lakes," *J. Geophys. Res.*, vol. 99, pp. 24527–24539, Dec. 1994.

[11] J.-F. Crétaux *et al.*, "SOLS: A lake database to monitor in the near real time water level and storage variations from remote sensing data," *Adv. Space Res.*, vol. 47, no. 9, pp. 1497–1507, May 2011.

[12] C. M. Birkett and B. Beckley, "Investigating the performance of the Jason-2/OSTM radar altimeter over lakes and reservoirs," *Mar. Geodesy*, vol. 33, no. 1, pp. 204–238, Aug. 2010.

[13] C. Hwang *et al.*, "Multi-decadal monitoring of lake level changes in the Qinghai-Tibet Plateau by the TOPEX/Poseidon-family altimeters: Climate implication," *Remote Sens.*, vol. 8, no. 6, p. 446, May 2016.

[14] Q. Huang *et al.*, "An improved approach to monitoring Brahmaputra river water levels using retracked altimetry data," *Remote Sens. Environ.*, vol. 211, pp. 112–128, Jun. 2018.

[15] S. Biancamaria *et al.*, "Satellite radar altimetry water elevations performance over a 200 m wide river: Evaluation over the Garonne River," *Adv. Space Res.*, vol. 59, no. 1, pp. 128–146, Jan. 2017.

[16] J. S. Da Silva, S. Calmant, F. Seyler, O. C. R. Filho, G. Cochonneau, and W. J. Mansur, "Water levels in the Amazon basin derived from the ERS 2 and ENVISAT radar altimetry missions," *Remote Sens. Environ.*, vol. 114, no. 10, pp. 2160–2181, Oct. 2010.

[17] T. V. Martin, H. J. Zwally, A. C. Brenner, and R. A. Bindschadler, "Analysis and retracking of continental ice sheet radar altimeter waveforms," *J. Geophys. Res., Oceans*, vol. 88, no. C3, pp. 1608–1616, 1983.

[18] S. Laxon, "Sea ice altimeter processing scheme at the EODC," *Int. J. Remote Sens.*, vol. 15, no. 4, pp. 915–924, Mar. 1994.

[19] C. H. Davis, "A robust threshold retracking algorithm for measuring ice-sheet surface elevation change from satellite radar altimeters," *IEEE Trans. Geosci. Remote Sens.*, vol. 35, no. 4, pp. 974–979, Jul. 1997.

[20] M. Passaro, P. Cipollini, S. Vignudelli, G. D. Quartly, and H. M. Snaith, "ALES: A multi-mission adaptive subwaveform retracker for coastal and open ocean altimetry," *Remote Sens. Environ.*, vol. 145, pp. 173–189, Apr. 2014.

[21] J. F. Beckers, J. A. Casey, and C. Haas, "Retrievals of lake ice thickness from Great Slave Lake and Great Bear Lake using CryoSat-2," *IEEE Trans. Geosci. Remote Sens.*, vol. 55, no. 7, pp. 3708–3720, Jul. 2017.

[22] M. Ricko, M. Charon, B. James, A. Carton, and J. Cretaux, "Intercomparison and validation of continental water level products derived from satellite radar altimetry," *J. Appl. Remote Sens.*, vol. 6, no. 1, p. 3614, 2012.

[23] H. Villadsen, X. Deng, O. B. Andersen, L. Stenseng, K. Nielsen, and P. Knudsen, "Improved inland water levels from SAR altimetry using novel empirical and physical retrackers," *J. Hydrol.*, vol. 537, pp. 234–247, Jun. 2016.

[24] Q. Gao *et al.*, "Analysis of retrackers' performances and water level retrieval over the Ebro river basin using sentinel-3," *Remote Sens.*, vol. 11, no. 6, p. 718, Mar. 2019.

[25] D. Ganguly, S. Chander, S. Desai, and P. Chauhan, "A subwaveform-based retracker for multipeak waveforms: A case study over Ukai dam/reservoir," *Mar. Geodesy*, vol. 38, no. 1, pp. 581–596, Sep. 2015.

[26] S. E. L. Howell, L. C. Brown, K.-K. Kang, and C. R. Duguay, "Variability in ice phenology on Great Bear Lake and Great Slave Lake, Northwest Territories, Canada, from SeaWinds/QuikSCAT: 2000–2006," *Remote Sens. Environ.*, vol. 113, no. 4, pp. 816–834, Apr. 2009.

[27] M. K. Woo *et al.*, "Science meets traditional knowledge: Water and climate in the Sahtu (Great Bear Lake) region, Northwest Territories, Canada," *Arctic*, vol. 60, no. 1, pp. 37–46, 2007.

[28] C. Bouzinac, *Cryosat Product Handbook*. Paris, France: European Space Agency, 2013.

[29] D. J. Wingham *et al.*, "Cryosat: A mission to determine the fluctuations in Earth's land and marine ice fields," *Adv. Space Res.*, vol. 37, no. 4, pp. 841–871, 2006.

[30] N. Picot, K. Case, S. Desai, P. Vincent, and E. Bronner, "AVISO and PODAAC user handbook," IGDR, GDR Jason Products, Mumbai, India, Tech. Rep. SMM-MU-M5-OP-13184-CN (AVISO) JPL D-21352 (PODAAC), 2008.

[31] D. J. Wingham, C. G. Rapley, and H. Griffiths, "New techniques in satellite altimeter tracking systems," in in *Proc. Int. Geosci. Remote Sens. Symp. Dig. (IGARSS)*, 1986, pp. 1339–1344.

[32] Y. Yang, C. Hwang, H.-J. Hsu, E. Dongchen, and H. Wang, "A subwaveform threshold retracker for ERS-1 altimetry: A case study in the Antarctic ocean," *Comput. Geosci.*, vol. 41, pp. 88–98, Apr. 2012.

[33] D. Schröder, D. L. Feltham, M. Tsamados, A. Ridout, and R. Tilling, "New insight from CryoSat-2 sea ice thickness for sea ice modelling," *Cryosphere*, vol. 13, no. 1, pp. 125–139, Jan. 2019.

[34] M. N. O. Sadiku, "Refractive index of snow at microwave frequencies," *Appl. Opt.*, vol. 24, no. 4, pp. 572–575, 1985.

[35] S. G. Warren and R. E. Brandt, "Optical constants of ice from the ultraviolet to the microwave: A revised compilation," *J. Geophys. Res.*, vol. 113, no. D14, pp. 1–10, 2008.

Yuande Yang received the M.S. degree in solid geophysics and the Ph.D. degree in geodesy and geomatics from Wuhan University, Wuhan, China, in 2006 and 2010, respectively.

From 2019 to 2020, he was a Visiting Scholar with Newcastle University, Newcastle upon Tyne, U.K. He is an Associate Professor with the Chinese Antarctic Center of Surveying and Mapping, Wuhan University. His research interests include the applications of satellite altimetry, Gravity Recovery and Climate Experiment (GRACE) and Global Navigation Satellite System (GNSS). His work consists of inland water level monitoring, mass balance of ice sheets, and land subsidence monitoring.

Philip Moore received the B.S. degree in mathematical science from Birmingham University, Birmingham, U.K., in 1972, and the Ph.D. degree from Brunel University, London, U.K., in 1976.

He was with the Department of Mathematics and Department of Civil Engineering, Aston University, Birmingham. He joined Newcastle University, Newcastle upon Tyne, U.K., in September 1999, as a Professor of Space Geodesy as part of the Geomatics Group. His research concentrates on mathematical and computational geodesy to multidisciplinary aspects including precise navigation, geophysical inferences from satellite orbital perturbations, mass redistribution and gravity field studies from dedicated gravity field missions, and global hydrology for ungauged basins using remote sensing.

Zhenhong Li received the B.S. degree in geodesy from Wuhan University, Wuhan, China, in 1997, and the Ph.D. degree in GPS, geodesy, and navigation from University College London, London, U.K., in 2005.

He is a Professor of imaging geodesy with the College of Geological Engineering and Geomatics, Chang'an University, Xi'an, China. He has over 20 years of research experience in space geodesy and remote sensing [mainly synthetic aperture radar interferometry (InSAR) and Global Navigation Satellite System (GNSS)] and their application to geohazards (e.g., earthquakes, landslides, and land subsidence) and precision agriculture. He specializes in the development of InSAR atmospheric corrections and time-series algorithms for precisely mapping surface movements, and he has made several original contributions to the direct estimation and/or mitigation of the effects of atmospheric water vapor on satellite radar measurements. He is a Principal Investigator of the Generic Atmospheric Correction Online Service for InSAR (GACOS).

Prof. Li is a Fellow of the International Association of Geodesy and an Associate Editor of *Advances in Space Research and Remote Sensing*.

Fei Li received the M.S. degree in geophysics from the University of Science and Technology of China, Hefei, China, in 1982, and the Ph.D. degree in solid geophysics from the Institute of Geodesy and Geophysics, Chinese Academy of Sciences, Wuhan, China, in 1992.

He joined Wuhan University, Wuhan, in August 1995, as a Professor of Geodesy. His principal research interests include the use of remote sensing and Global Navigation Satellite System (GNSS) for monitoring changes in the Earth and planets.